Accepted Manuscript

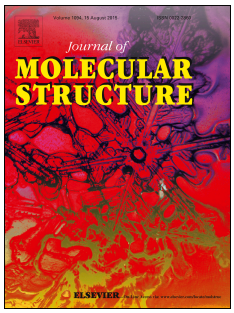

Insights into the nature of weak noncovalent interactions in 3-(4-fluorophenyl)-6-(2-fluorophenyl)-1,2,4-triazolo[3,4-*b*][1,3,4]thiadiazole, a potential bioactive agent: X-ray, QTAIM and molecular docking analysis

Lamya H. Al-Wahaibi, Gopalan Akilandeswari, Ravisankar Anusha, Nora H. Al-Shaalan, Omkulthom M. Alkmali, Ali A. El-Emam, Judith M. Percino, Subbiah Thamotharan

PII: S0022-2860(19)30124-3

DOI: https://doi.org/10.1016/j.molstruc.2019.01.106

Reference: MOLSTR 26157

To appear in: *Journal of Molecular Structure*

Received Date: 28 December 2018

Revised Date: 29 January 2019

Accepted Date: 31 January 2019

Please cite this article as: L.H. Al-Wahaibi, G. Akilandeswari, R. Anusha, N.H. Al-Shaalan, O.M. Alkmali, A.A. El-Emam, J.M. Percino, S. Thamotharan, Insights into the nature of weak noncovalent interactions in 3-(4-fluorophenyl)-6-(2-fluorophenyl)-1,2,4-triazolo[3,4-*b*][1,3,4]thiadiazole, a potential bioactive agent: X-ray, QTAIM and molecular docking analysis, *Journal of Molecular Structure* (2019), doi: https://doi.org/10.1016/j.molstruc.2019.01.106.

GRAPHICAL ABSTRACT

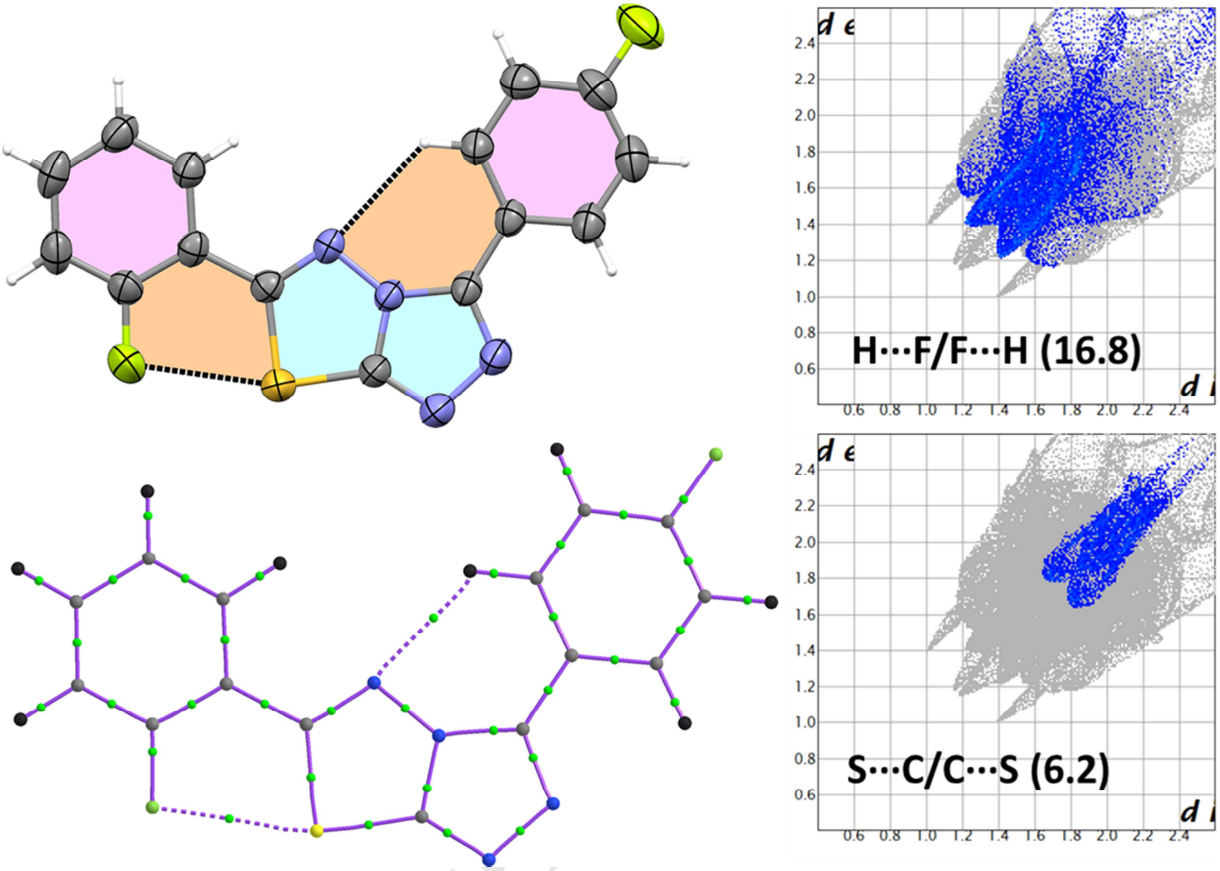

Insights into the nature of weak noncovalent interactions in 3-(4-fluorophenyl)-6-(2-fluorophenyl)-1,2,4-triazolo[3,4-*b*][1,3,4]thiadiazole, a potential bioactive agent: X-ray, QTAIM and molecular docking analysis

Lamya H. Al-Wahaibi[a], Gopalan Akilandeswari[b], Ravisankar Anusha[b], Nora H. Al-Shaalan[a], Omkulthom M. Alkmali[c], Ali A. El-Emam[d], Judith. M. Percino[e], Subbiah Thamotharan[b,*]

[a] *Department of Chemistry, College of Sciences, Princess Nourah Bint Abdulrahman University, Riyadh 11671, Saudi Arabia*

[b] *Biomolecular Crystallography Laboratory, Department of Bioinformatics, School of Chemical and Biotechnology, SASTRA Deemed University, Thanjavur-613 401, India*

[c] *Department of Pharmaceutical Sciences, College of Pharmacy, Princess Nourah Bint Abdulrahman University, Riyadh 11671, Saudi Arabia*

[d] *Department of Medicinal Chemistry, Faculty of Pharmacy, University of Mansoura, Mansoura 35516, Egypt*

[e] *Unidad de Polímeros y Electrónica Orgánica, Instituto de Ciencias, Benemérita Universidad Autónoma de Puebla, Val3-Ecocampus Valsequillo, Independencia O2 Sur 50, San Pedro Zacachimalpa, Pue. Mexico*

Corresponding author.

E-mail address: thamu@scbt.sastra.edu (S. Thamotharan).

ABSTRACT

A thorough examination of weak interactions present in the crystal structure of the title compound was investigated. Intramolecular C–H···N and F···S interactions make the molecule as fused 6,5,5,5,6,6-membered ring system. Two of the closely related structures show 1D-isostructurallity with the title compound. The crystal structure is stabilized by different types of weak intermolecular C–H···N, C–H···F, C–H···π and S···π and π···π interactions. The first two strongest dimers are stabilized by stacking interactions. The nature of these interactions and their role was established through quantum theory of atoms-in-molecules approach. The Hirshfeld surface analysis clearly reveals that the *para*-substituted fluorine substantially change the contribution of intermolecular H···H and H···C contacts. The molecular docking analysis suggests that the title compound shows anti-inflammatory activity and selective against cyclooxygenase-1 (COX-1) enzyme and the 2-fluorophenyl and triazole moieties of the title compound are involved in the π···π interactions with active site aromatic residues.

Keywords: 1,2,4-Triazolo[3,4-*b*][1,3,4]thiadiazole; anti-inflammatory; PIXEL; QTAIM; Molecular docking

1. Introduction

Non-covalent interactions between molecules play a vital role in supramolecular chemistry, structural biology and materials science [1]. A thorough investigation of both strong and weak non-covalent interactions is an essential aspect of crystal engineering as it assists to tailor new materials with desired physicochemical properties [2-4]. The role of conventional hydrogen bonds and π···π interactions is well recognized in crystal engineering [5-7], structural chemistry and biology [8]. The importance of different types of weak interactions in classical and non-classical nature in different organic materials was studied using X-ray crystallography and a variety of theoretical approaches [9-12]. In order to understand the importance of different weak interactions including halogen bonds in a pharmaceutically active triazolothiadiazole derivative, we synthesized one of the triazolothiadiazole derivatives bearing two fluorine atoms and its crystal structure has been explored by single crystal X-ray diffraction.

The title compound possesses two azoles namely 1,2,4-triazole and 1,3,4-thiadiazole and each of this azole has their own importance in different fields such as medicinal

chemistry, agriculture and industrial applications. The fused products of these two azoles possess versatile biological activities including anti-inflammatory [13,14], antimicrobial [13], anticancer [15], analgesic [16], antioxidant [17] and antifungal [18] activities. Some of the triazolothiadiazoles were also discovered as selective inhibitors of the c-Met kinase [19]. The Cambridge Structural Database (CSD) search (version 5.39 updates August 2018) disclosed that there are 64 hits containing 3,6-disubstituted-1,2,4-triazolo-1,3,4-thiadiazole derivatives of which 8 hits (Fig. 1) found with phenyl moiety substituted at the 3 and 6 positions of the fused triazolothiadiazole (CSD reference codes: HODNOE [20], ILETOK [21], KOFKOG [22], RAPSUX [23], ROGGIE [24], XERZUQ [25], VEGVAE [26] and LEPQED [27]).

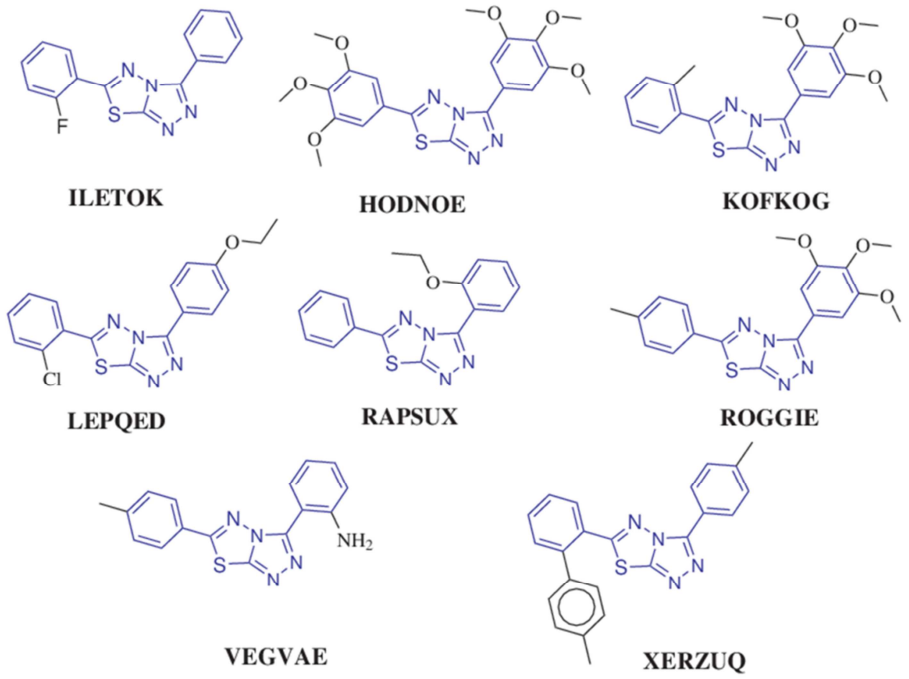

Fig. 1. Chemical structures of closely related analogs of the title compound.

In the present investigation, we used different theoretical approaches (PIXEL, quantum theory of atoms-in-molecules (QTAIM), and molecular electrostatic potential and Hirshfeld surface analysis) to study the weak intermolecular interactions existing in the title compound. The PIXEL method was used to evaluate the intermolecular interaction energies of different molecular pairs in the crystal structure of the title compound. Lattices energies were also calculated using the same code for the title compound and its closely related structures to understand the nature of crystal packing. The quantitative molecular electrostatic potential surface was computed to identify the potential sites involved in the intermolecular interactions in the crystal structure of the title compound. Further, Hirshfeld surface analysis

was performed to quantify the contribution of different intermolecular contacts in the title compound and its closely related structures and to delineate the role of fluorine substitutions in the title compound. The topological properties of different weak interactions were computed based on the Bader's QTAIM approach [28]. In order to assess the potential bioactivities of the title compound, we performed *in-silico* docking of the title compound against different targets such as *Ovis aries* cyclooxygenase-1 (COX-1), *Homo sapiens* cyclooxygenase-2 (COX-2) and lanosterol 14α-demthylase of *Mycobacterium tuberculosis* (*Mtb*CYP51) and *Candida albicans* (*Ca*CYP51).

2. Experimental

2.1. Synthesis and crystallization

The title compound was synthesized starting with 4-fluorobenzohydrazide (**1**) following the reaction sequences outlined in Scheme 1. A mixture of 4-amino-5-(4-fluorophenyl)-4*H*-1,2,4-triazole-3-thiol **3** (2.1 g, 0.01 mol), 2-fluorobenzoyl chloride (1.40 g, 0.01 mol) and phosphorous oxychloride (10 mL) was heated under reflux for two hours. On cooling, the reaction mixture was cautiously poured onto crushed ice (50 gm) and the precipitated solid product was filtered, washed with saturated sodium hydrogen carbonate solution and then with water, dried crystallized from ethanol to yield 2.42 g (77%) of the title compound **(A)**. M.p. 172-174 ^{o}C (445-447 K) as colourless fine needle crystals. Suitable XRD single crystals were obtained by slow evaporation of chloroform-ethanol solution (1:1) at room temperature. ^{1}H NMR ($CDCl_3$, 500.13 MHz): δ 7.16-7.25 (m, 4H, Aromatic-H), 7.31-7.33 (m, 2H, Aromatic-H), 7.54-7.56 (m, 2H, Aromatic-H). ^{13}C NMR ($CDCl_3$, 125.76 MHz): δ 115.11, 115.92, 116.21, 120.73, 124.27, 127.54, 127.77, 133.45, 144.57, 158.43, 161.96 (Aromatic-C), 160.05 (C-3), 160.46 (C-8), 163.96 (C-6).

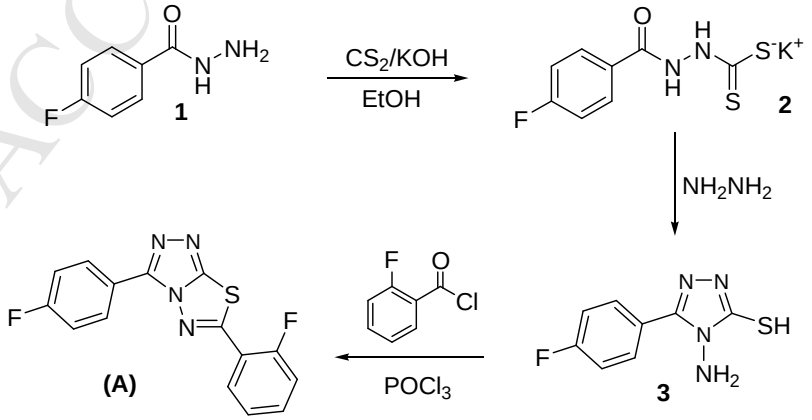

Scheme 1. Synthesis of the title compound.

2.2. Single crystal X-ray diffraction (SCXRD)

The X-ray intensity data were measured from single crystal of the title compound on a Bruker APEK-II CCD diffractometer with monochromatic Mo $K\alpha$ (λ = 0.71073 Å) radiation at room temperature (293(2) K). Data reduction and the refinement of cell parameters were performed using the program SAINT (Bruker AXS, 2014). The absorption correction was applied using the multiscan method [29] implemented in the program SADABS (Bruker AXS, 2014). The structure of the title compound was solved by the direct methods using the program SHELXS-97 [30] and the structure was refined using the SHELXL-2017/4 program [31]. The non-hydrogen atoms were refined anisotropically and the hydrogen atoms were placed in idealized geometry using riding model with C-H=0.93 Å and $U_{iso}(H)=1.2U_{eq}(C)$. Highly disordered solvent (possibly water) was present in the channels parallel to the crystallographic *c* axis. Since the disordered solvent molecules could not be identified, the SQUEEZE routine of PLATON [32] was used to remove the effects of approximately 12 electron equivalents from 183 $Å^3$ of potential solvent area volume. Crystal data, data collection and structure refinement parameters are summarized in Table 1. The molecular dimers were drawn using the program MERCURY [33].

2.3. Computational details

Crystal structure geometry of the title compound was used as a starting model for geometry optimization and followed by vibrational frequency calculation. The optimized structure was found to be minima with no imaginary frequency. Both calculations were performed in the gas-phase with M06-2X/cc-pVTZ level of theory [34] using the Gaussian09 program [35]. Grimme's empirical dispersion (D3) correction was included in all calculation [36].

The Hirshfeld surface and the decomposed 2D fingerprint plots were generated for the title compound and its closely related structures using CrystalExplorer package [37] in order to analyze intermolecular interactions present in these structures. Further, we carried out PIXEL calculation [38,39] to evaluate the strengths of various molecular pairs held by different types of intermolecular interactions in the title compound and its closely related structures. The lattice energy was also computed for these structures using PIXEL method which partitioned into the Coulombic, polarization, dispersion and repulsion energy terms. We successfully utilized the above two approaches for different systems and the details were previously published [12, 40-45]. Using the PIXEL calculation, we identified energetically

significant molecular pairs were identified. Furthermore, XPAC2.0 program [46,47] was used to identify the common packing features present between the title compound and its closely related structures. The quantitative molecular electrostatic potential map was constructed and visualized on the three dimensional surface using the program WFA-SAS [48].

Further, the interaction energies (ΔE_{CP}) for these dimers were computed at their crystal structure geometry with normalized bond lengths involving hydrogen atoms with M06-2X-D3/cc-pVTZ level of theory. The ΔE_{CP} energies were corrected for basis-set superposition error (BSSE) using the counterpoise correction method proposed by Boys and Bernardi [49]. For the above molecular pairs, the topological properties were calculated using an approach of quantum theory of atoms-in-molecules (QTAIM) from AIMALL package [50]. The dissociation energy (DE_{int}) for the interaction was estimated through an empirical formula proposed by Espinosa-Molins-Lecomte [51].

2.4. Molecular docking analysis

The anti-inflammatory, antimicrobial and antifungal activities of the title compound was investigated by *in silico* molecular docking against different targets such as cytochrome P450 lanosterol-14α-demethylases (CYP51) of *Mycobacterium tuberculosis* (pdbid: 1EA1) and *Candida albicans* (pdbid: 5V5Z) and two cyclooxygenases (*Ovis aries* COX-1, pdbid: 1EQG and *Homo sapiens* COX-2, pdbid: 5IKR). The preparation of protein and the ligand molecules for the docking study was carried out as mentioned in our earlier report [12] using the Schrödinger suite (Schrödinger Release 2016-3, LLC, New York, NY, 2016). The binding energies of the docked pose of the compounds were calculated using the glide extra precision (Glide XP) scoring scheme implemented in the Glide module [52]. To compare the binding affinity of the title compound, we used different standard inhibitors: ibuprofen (COX-1), mefenamic acid (COX-2) and Flucanazole (CYP51).

3. Results and discussion

3.1. Structural description

The title compound crystallizes in the tetragonal system with the space group of $I4_1/a$ and one molecule present in the asymmetric unit. The compound comprises four ring systems, two six-membered (4-fluorophenyl and 2-fluorophenyl) and two fused five-membered rings (thiadiazole and 1,2,4-triazole). In the solid state, the overall conformation of the molecule is completely planar and rings are coplanar with each other as evident from the dihedral angles

(2.5-7.3°) formed by the mean planes of these rings and the torsion angles T1 and T2 (Fig. 2). It should be noted that the two intramolecular contacts (H15···N4 and F1···S1) provide support to maintain the planarity and rigidity of the molecule in the crystalline state and make the molecule as fused pseudo 6,5,5,5,6,6-membered ring system (Fig. 2).

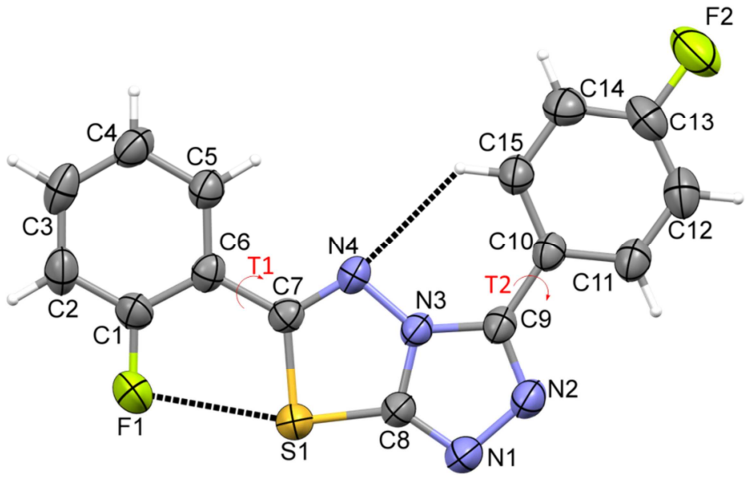

Fig. 2. ORTEP diagram showing intramolecular C–H···N and F···S interactions in the title compound along with atom-numbering scheme.

3.2. Conformational analysis and quantitative analysis of intramolecular interactions

In order to assess the role of above mentioned intramolecular contacts, we performed rigid potential energy surface (PES) scan for the two torsion angles (T1 and T2) which involve the rotation of terminal phenyl rings. The rigid PES scan was performed using B3LYP/6-31+G(d) level of theory for these torsion angles separately from -180 to 180° with the increment of 5°. The result suggests that the minimum energy conformer is found to be at 5° for T1 and 0° for T2 torsion angles (Fig. S1). These angles are close to the X-ray geometry of title compound which favor the formation of intramolecular H15···N4 and F1···S1 contacts. Further, the molecule of title compound was fully optimized without any geometrical constraints as mentioned in the experimental section. The optimized structure was found to be very close to the X-ray structure. The root mean squared deviation (RMSD) between X-ray and the optimized structures was calculated to be 0.12 Å. This result is also suggesting the importance of intramolecular interactions in the stabilization of planar molecular conformation of title compound.

To retrieve closely related structures of the title compound, we performed CSD search using the chemical structure of the title compound with the exclusion of fluorine substituents

as a template. This search yielded 8 hits and their chemical structures are depicted in Fig. 1. To compare the conformation of title compound with its closely related known structures, two important torsion angles (T1 and T2) which describe the conformation of these molecules are used (Table S1) and the dihedral angles are formed between phenyl rings attached to the central rings with respect to the mean plane of central triazolothiadiazole ring summarized (Table S2).

Further, atoms of central two five-membered rings are used for structural superimposition of the title compound with its closely related structures to see the effect of substituents on phenyl rings (Fig. S2). These analyses collectively indicate that the 2-ethoxy moiety in RAPSUX [53] affect the planarity of the molecule. The 2-ethoxy substituted phenyl is oriented at an angle of 49° with respect to the mean plane of the central triazolothiadiazole ring. This deviation is likely due to the absence of intramolecular contact between 2-ethoxyphenyl and the N atom of thiadiazole ring. It should be noted that the effect of substituents on phenyl ring attached to the thiadiazole ring on the conformation is marginal.

Further, we present a detailed analysis of topological properties of intramolecular interactions at the BCP in the crystalline geometry of title compound and its closely related structures based on the QTAIM approach. The topological properties for intramolecular interactions (C–H···N and S involving contact) in these structures are summarized in Table 2 (a complete details are given in Table S3) and the molecular graphs showing the intramolecular interactions are illustrated in Fig. S3. The analysis of the topological properties for these intramolecular interactions suggests that the intramolecular C–H···N interaction as found in the structure of title compound is invariant except in RAPSUX structure [53]. This absence is due to the presence of ethoxy group at the *ortho* position of the phenyl ring attached to the triazole ring. The dissociation energy (DE_{int}) for these interactions ranging from 2.08 (LEPQED [27] to 3.22 kcal mol^{-1} (HODNOE [20]). However, the ethoxy O makes an intramolecular interaction (O1···N1) with the N atom of the thiadiazole moiety with DE_{int} of 1.92 kcal mol^{-1}. It should be noted that these C–H···N interactions show the trend of exponential decay (with $R^2 > 0.99$) in the magnitude of electron density (ρ) and the Laplacian of electron density ($\nabla^2\rho$) with increasing length of the bond path (Fig. S4).

Moreover, the S atom is participating in an intramolecular contact in five structures. The F/Cl···S contact is observed in three structures (**A**, ILETOK and LEPQED) and in another two structures, H/C···S interactions were observed. The strongest S involving interaction is found to be F···S in (**A**) with DE_{int} of 4.25 kcal mol^{-1}. A slight rotation of

phenyl ring attached to thiadiazole ring in ROGGIE, RAPSUX, HODNOE and VEGVAE structure avoids the formation of S involving intramolecular contact. It is also to be noted that the $|V(r)|/G(r)$ ratio is calculated to be less than one for all the intramolecular contacts, comparable to those reported for other hydrogen bonds [54].

3.3. Molecular dimers in the crystal structure

The crystal structure of the title compound **A** can be described as four units of dimer (Fig. 3) and this dimer (motif **III**) is formed by intermolecular C–H···N interactions. The adjacent dimers are interconnected by S··π contacts (motif **IV**). Further, the energetically significant dimeric pairs were identified from the PIXEL energy calculation. The results suggest that there are six dimers (**I-VI**) which are held together by different intermolecular interactions (Table 3 and Fig. 4). The interactions energies (ΔE_{CP}) for these dimers were further evaluated by DFT method as mentioned in the experimental section. It should be mentioned that the interaction energies (E_{tot} and ΔE_{CP}) of dimers calculated by PIXEL and DFT methods are comparable.

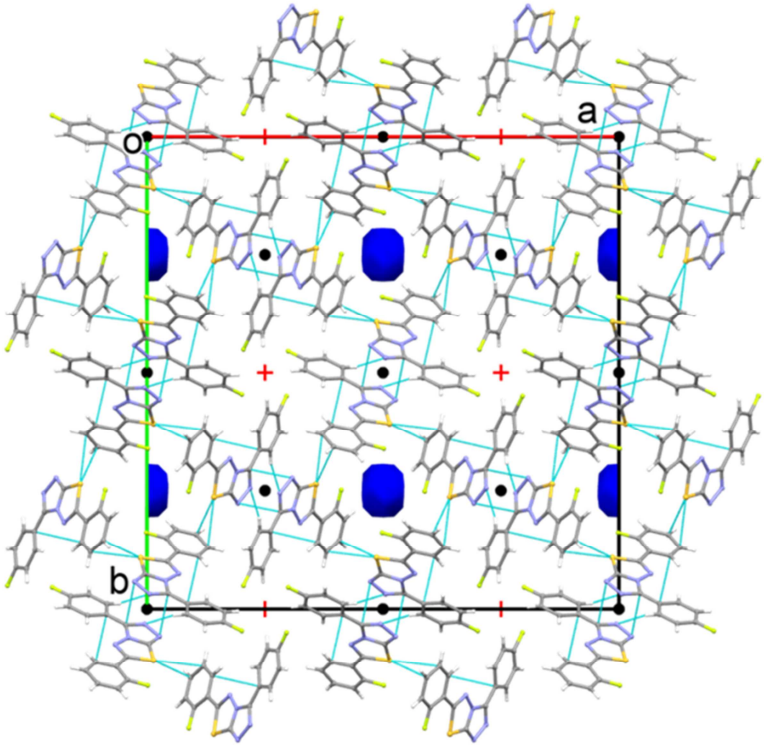

Fig. 3. Crystal structure of the title compound viewed down the *c* axis. The voids are indicated as blue spheres. The symbol '+' and small black spheres denote the 4_1 screw axis and center of inversion, respectively.

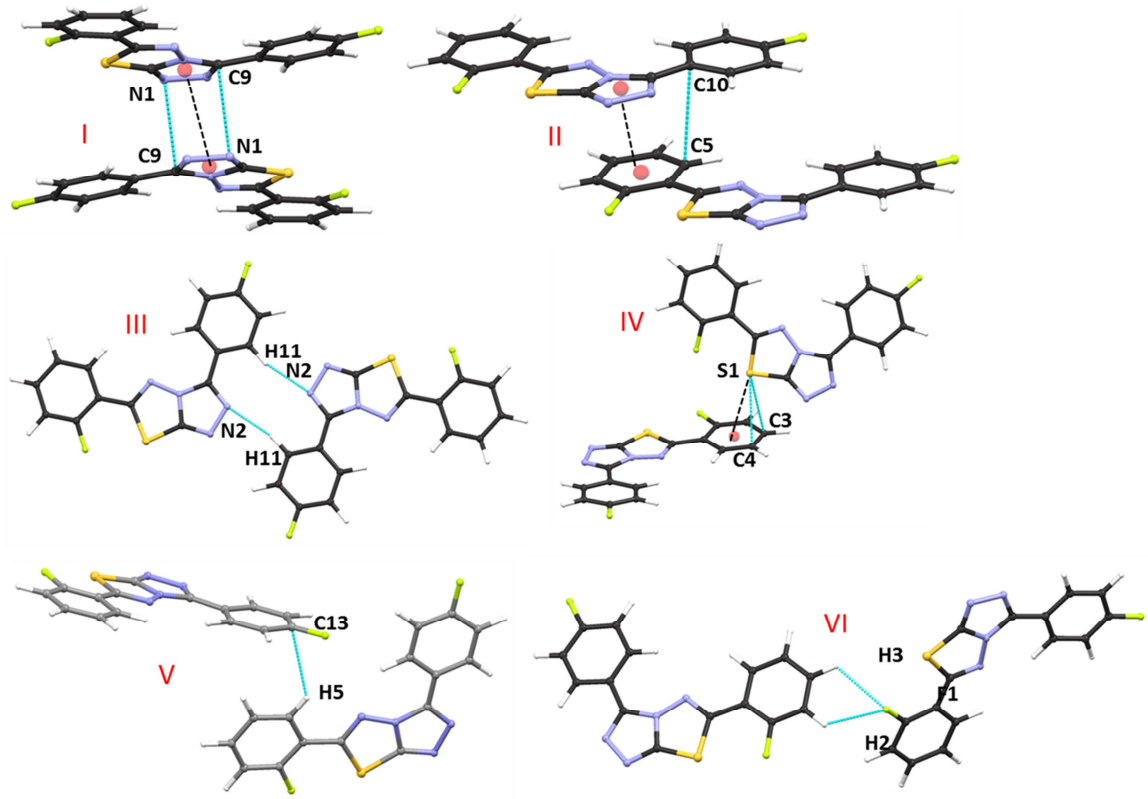

Fig. 4. Molecular dimers observed in the crystal structure of the title compound. The ring centroid position is shown as small red sphere.

The molecular dimer **I** is formed by stacking of adjacent triazole rings related by center of inversion with an E_{tot} value of -9.2 kcal mol^{-1}. The distance between the centroids of the triazole ring is being 3.317(3) Å. The electrostatics and dispersive energy components are contributing 34% and 66% towards the stabilization of this dimer. Further, to confirm the existence and to quantify this stacking interaction, we performed QTAIM analysis. The molecular graphs showing the presence of different intermolecular interactions in various molecular pairs observed in the title compound are illustrated in Fig. S5 and the topological properties for these intermolecular interactions are summarized in Table 4. In dimer **I**, two symmetrical contacts (four BCPs in total) are presented between this dimer. One of the contacts involved between N1 and C9, while the second contact is formed between N2 and N3. The DE_{int} for these contacts are nearly equal (0.95 and 0.92 kcal mol^{-1}) in strength.

The second strongest molecular pair **II** is established by molecular stacking between adjacent molecules (E_{tot} = -8.4 kcal mol^{-1} with the contribution of 83% dispersive energy towards the stabilization). There is a C5···C10 ($\pi\cdots\pi$) contact observed between adjacent molecules and the centroid-to-centroid distance (3.664(3) Å) between the triazole and 2-

fluorophenyl rings supports for the formation in π···π interaction. QTAIM calculation reveals that there are four (3, -1) bond critical points observed (N···C and C···C atom pairs) between atoms and confirms the existence of π···π stacking interactions between the molecular pair of **II**. The DE_{int} for these contacts ranging from 0.50 to 0.71 kcal mol^{-1}.

The centrosymmetric dimer **III** is formed *via* intermolecular C–H···N interactions (involving H11 and N2 atoms). These interactions generate a closed $R_2^2(10)$ loop and the interaction energy for this dimer calculated by the PIXEL method is being -7.1 kcal mol^{-1}. For the stabilization, the electrostatic energy (59%) is contributing more when compared to the dispersion energy (41%) component. The topological analysis confirms the presence of these closed loop structure with the DE_{int} for each H···N contact is found to be 2.20 kcal md^{-1}.

The dimer **IV** is primarily stabilized by intermolecular S···π interaction and there are non-bonded contacts observed between S1 atom and C atoms (C3 and C4) of the 2-fluorophenyl ring. The intermolecular interaction energy (E_{tot}) for this dimer is calculated to be -4.9 kcal mol^{-1}. The electrostatic (49%) and dispersion (51%) energies are contributing nearly equal towards the stabilization of this molecular pair. The distance between S1 and the centroid of the 2-fluorophenyl ring is 3.521(3) Å. This dimer was further subjected to QTAIM analysis to delineate the nature of interactions present between molecules. The result exposes the existence of S···π interactions with DE_{int} for these contacts are 0.87 and 0.91 kcal mol^{-1}. It is important to note that there is an intermolecular C–H···N (BCP between H3 and N1 atoms) interaction which displays a significant role in the stabilization of this dimer. The DE_{int} for this contact (1.24 kcal mol^{-1} is slightly stronger than the S···π interactions.

Intermolecular C–H···π (involving H5 and C13 atoms) interaction stabilizes the molecular pair **V** with the E_{tot} value of -4.3 kcal mol^{-1}. The stabilization of this dimer is essentially dispersive (73%) in nature. The topological analysis suggests that there are four BCPs observed in the molecular pair which confirms the existence of C–H···π interaction in addition to the weak intermolecular C–H···F interactions (Table 4 and Fig. S5). The C–H···π interactions are slightly weaker than one of the C–H···F interactions as evident from the dissociation energies for these interactions.

The dimer **VI** is held by intermolecular three-center C–H···F interactions which generate a loop. The E_{tot} value of this dimer is calculated to be -1.9 kcal mol^{-1} and this motif is stabilized by predominantly dispersive in nature (73%). According to QTAIM analysis, the presence of these interactions are confirmed through the (3, -1) bond critical points between H and F atoms. The dissociation energy for these interactions were found to be 1.38 (H3···F1)

and 1.28 (H2···F1) kcal mol^{-1}. Overall, the results suggest that C–H···F interactions observed in motif **VI** is the second strongest interactions in the crystal structure of the title molecule (first strongest one is the C–H···N interaction observed in molecular pair **III**). It is worth mentioning that the magnitude of electron density values for all the interactions observed in different molecular pairs falls in the range [0.013 < ρ (e Å^{-3}) < 0.236] proposed by Koch and Popelier for H-bonds [55,56]. On the other hand, the magnitude of the Laplacian for C–H···N and C–H···F interactions falls within the suggested limit [0.580 < $\nabla^2\rho$ (e Å^{-5}) < 3.355]. The intermolecular C–H···N and C–H···F (involving *ortho* fluorine F1) interactions are displayed important roles as compared to other weak interactions (they are in non-classical nature) in the crystalline state as evident from the topological properties.

3.4. Hirshfeld surface (HS) analysis and 2D fingerprint plots (FP)

HS analysis was performed to gather decomposed 2D fingerprint plots for the title compound and its closely related structures to quantify the contribution of various intermolecular interactions in the respective crystal packing (Table S4). In the title compound, there are three short contacts namely C5···C10 (motif **II**) and H11···N2 (motif **III**) and S1···C3 (motif **IV**) are clearly visible on the HS and the H11···N2 contacts are appeared as bright red spots among them as shown in Fig. 5(a).

In order to understand the role of second fluorine atom (*para* substituted F) in the crystal packing, we compared the relative contributions of different intermolecular contacts in the title compound and its closely related structure, ILETOK (4H, fluorine absent at this position). From Fig. 5(b), one can clearly visualize the distinct fingerprint plots obtained for these two structures. Most importantly, the contribution of intermolecular H···F contacts are increased and there is a reduction of H···H (by 5.2%) and H···C/C···H (7.7%) in **A**, due to the presence of *para*-substituted fluorine. Another distinct feature observed between these two structures is the contribution of S···C/C···S contact which indicates the presence of S···π interaction. In case of compound **A**, S···C/C···S contacts contribute 6.2% to the total HS area and the corresponding contacts are contributing less than 2% in other closely related structures. This is clearly indicating that the S···π interaction is unique in the title compound. The intermolecular H···N/N···H, C···N/N···C and C···C contacts are comparable in these two structures and H···S/S···H contacts are almost 2 times greater in the case of ILETOK. As discussed in the previous section, the *para*-substituted fluorine (F2) stabilizes the motif **V** along with two H···C contacts as observed from the topological analysis. Overall, this

analysis indicates that *para*-substituted fluorine plays an important role in the crystal packing in addition to *ortho*-substituted fluorine. Intermolecular C···C contacts are contributing 5.2% to the total HS area and they are concentrated around $d_e = d_i = 1.8$ Å as green dots which demonstrate the existence of π stacking interactions in the title compound (**A**). Further, to confirm the presence of π stacking interactions, the HS was mapped with the shape index. In this diagram, the pattern of convex blue and concave red triangles reveal the existence of these interactions (Fig. S6).

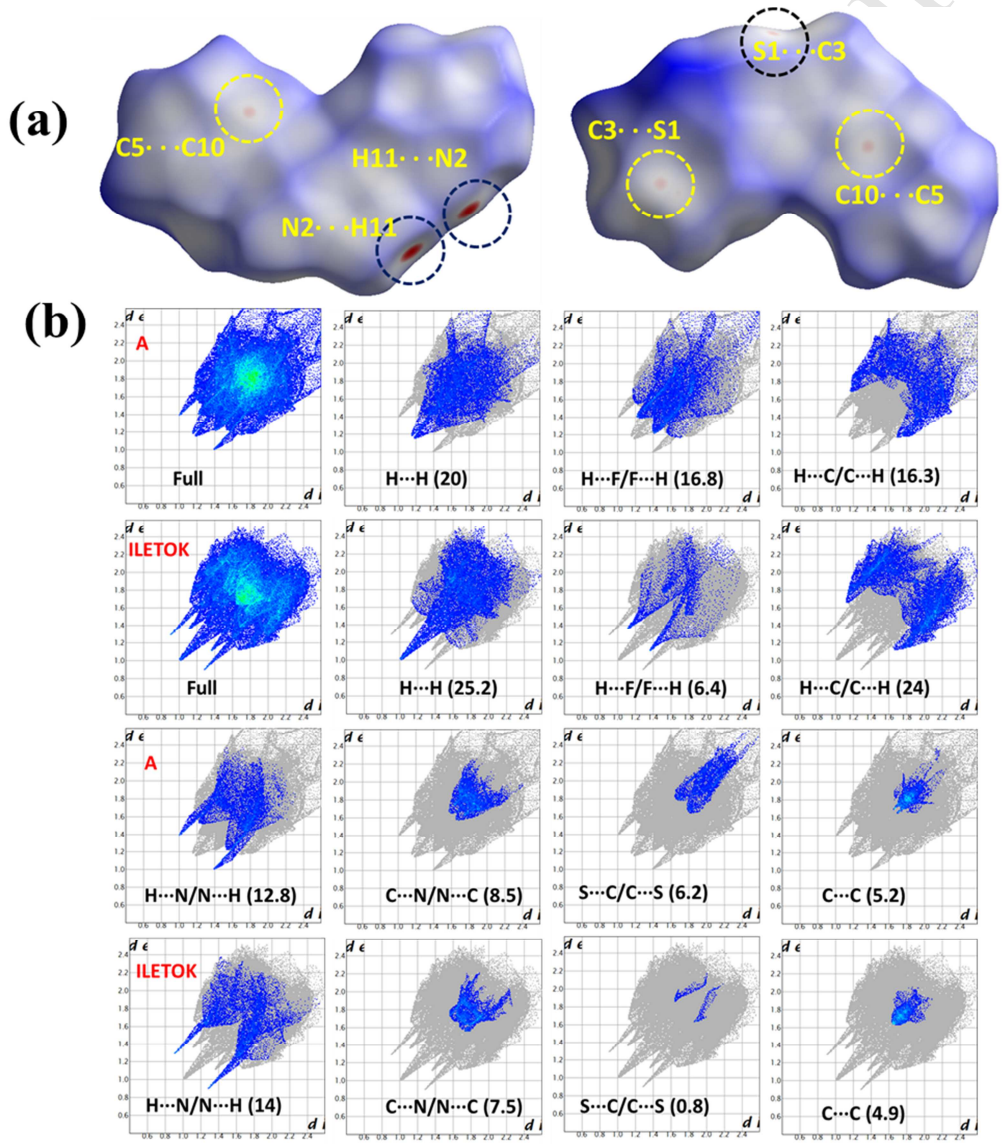

Fig. 5. (a) Two different views of Hirshfeld surfaces of the title compound **A** and short contacts are broken-circled and (b) the relative contributions of different intermolecular contacts to the total Hirshfeld surface area in **A** and its closely related structure ILETOK

3.5. Common packing features and lattice energies

Lattice energies were computed using the PIXEL method for the title compound **A** and its 8 closely related structures (Table S5). It is noted that the lattice energies for these molecules ranging from -32.2 (for title compound) to -47.1 kcal mol^{-1} (for HODNOE). The higher lattice energy can be attributed to the presence of voids in the crystals of the title compound. Moreover, the dispersion energy component is predominant (> 63%) towards the stabilization and the remaining comes from the electrostatic energy component in all cases. Further, the common packing features present between the title compound and its closely related structures were analyzed. As shown in Fig. S7, the compound **A** (**motif II**) shares one-dimensional isostructurality [46] only with ILETOK (dissimilarity index x =6.1 and stretch parameter D = 0.23 Å) and XERZUQ (dissimilarity index x =10.7 and stretch parameter D = 0.34 Å).

3.6. Quantitative molecular electrostatic potential

The quantitative molecular electrostatic potentials (MESP) for the title compound at its crystal structure geometry was analyzed to explore the electrostatic potential distribution and to understand the nature of interactions that exist in the crystal packing. The 0.001 au electron density isosurface of the title molecule of (**A**) is depicted in Fig. 6. The very strongly positive electrostatic potential of the 2-fluorophenyl hydrogen atoms ($V_{s,max}$ = 29.75 to 27.06 kcal mol^{-1}) and the negative potential ($V_{s,min}$ = -4.88 and -4.50 kcal mol^{-1}) around F1 indicates their propensities for hydrogen bonding. The positive electrostatic potential of the 4-fluorophenyl hydrogen atoms is relatively weaker as compared to 2-fluorophenyl hydrogen atoms and there is no σ-hole existing for the atom F1 as observed in a closely related structure ILETEK. In contrast, there is a σ-hole along the C13–F2 bond with the $V_{s,max}$ of -15.26 kcal mol^{-1} and the $V_{s,min}$ values of -16.86 and -16.79 kcal mol^{-1} which correspond to lone pairs of F2 atom. The nitrogen atoms (N1 and N2) of the triazole ring have strong negative potentials with $V_{s,min}$ values of -41.92 and -40.18 kcal mol^{-1}, respectively, and these two atoms are involved in the intermolecular interactions as evident from PIXEL and QTAIM analysis. The negative potential is observed for the lone pairs of S atom with $V_{s,min}$ values of 0.30 and 0.99 kcal mol^{-1}. It is of interest to note that there is a positive potential (σ-hole) with $V_{s,max}$ value of 16.01 kcal mol^{-1} which is approximately perpendicular to the position of lone pairs. This is clearly supports for the existence of motif **IV** in the title compound **A**.

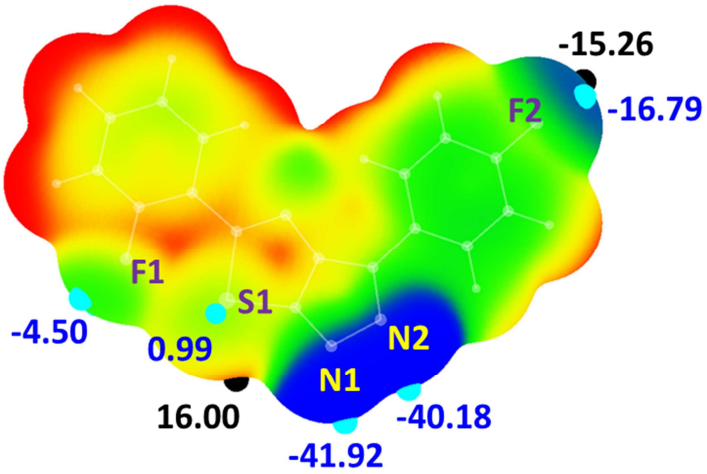

Fig. 6. Molecular electrostatic surface potentials of the title compound mapped over the electron density isosurface at 0.001 au. The positive ($V_{s,max}$) and negative ($V_{s,min}$) potentials are shown as small black and blue spheres, respectively.

3.7. Molecular docking analysis

The flexible ligand docking analysis revealed that the title compound may exhibit anti-inflammatory, antimicrobial and antifungal activities as compared to control drugs. The binding energies of the title compound (**A**) and control inhibitors for different targets are summarized in Table 5. The binding pose of compound (**A**) and control drugs along with their protein targets are depicted in Figs. 7 and S8-9. In both COX-1 and COX-2, the title compound (**A**) makes two important π···π stacking interactions with residues Tyr 385 and Trp 387 through its 2F-phenyl ring. The residue Tyr 355 is also forming a stacking interaction with the triazole ring of the compound (**A**) in the case of COX-1. It should be noted that compound (A) is slightly more selective towards COX-1. Compound (**A**) binds with higher affinity with both *Mtb*CYP51 and *Ca*CYP51 targets as compared to the control inhibitor antifungal drug fluconazole. In *Mtb*CYP51, again the 2F-phenyl ring of the title compound involved in stacking interaction with Tyr 76 residue. The same residue is also participating in stacking interaction with the triazole ring of the fluconazole inhibitor.

(a)

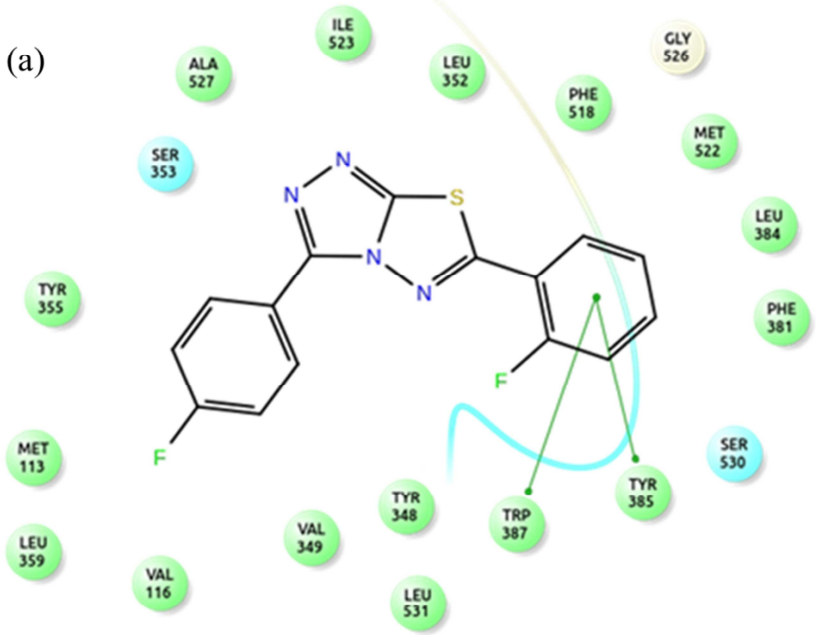
ILE 523
ALA 527
LEU 352
GLY 526
PHE 518
SER 353
MET 522
LEU 384
TYR 355
PHE 381
MET 113
SER 530
TYR 348
TYR 385
TRP 387
VAL 349
LEU 359
VAL 116
LEU 531
N
N
N
N
S
F
F

(b)

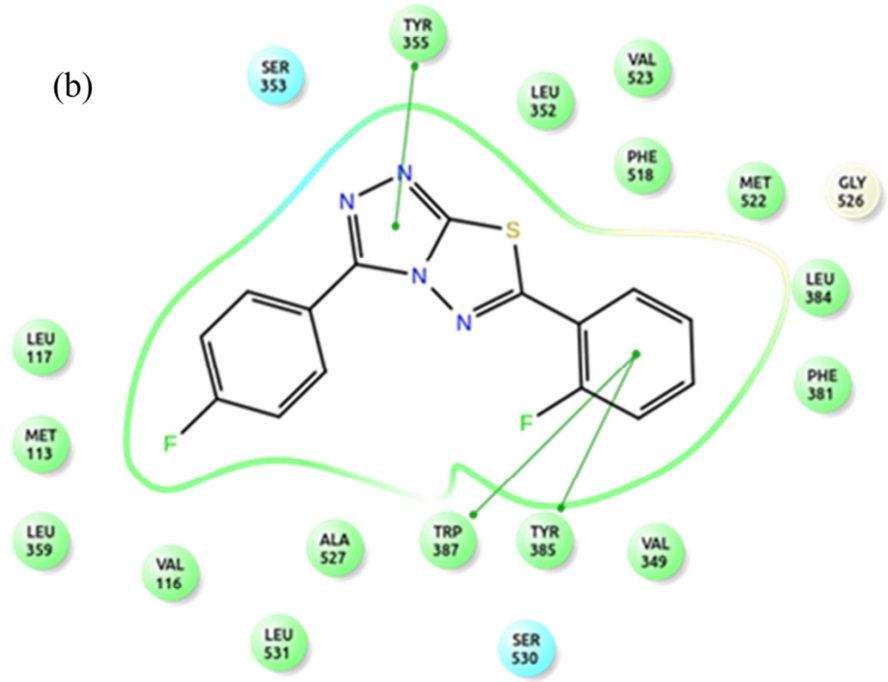
TYR 355
SER 353
VAL 523
LEU 352
PHE 518
MET 522
GLY 526
LEU 384
LEU 117
PHE 381
MET 113
LEU 359
ALA 527
TRP 387
TYR 385
VAL 349
VAL 116
LEU 531
SER 530
N
N
N
S
F
F

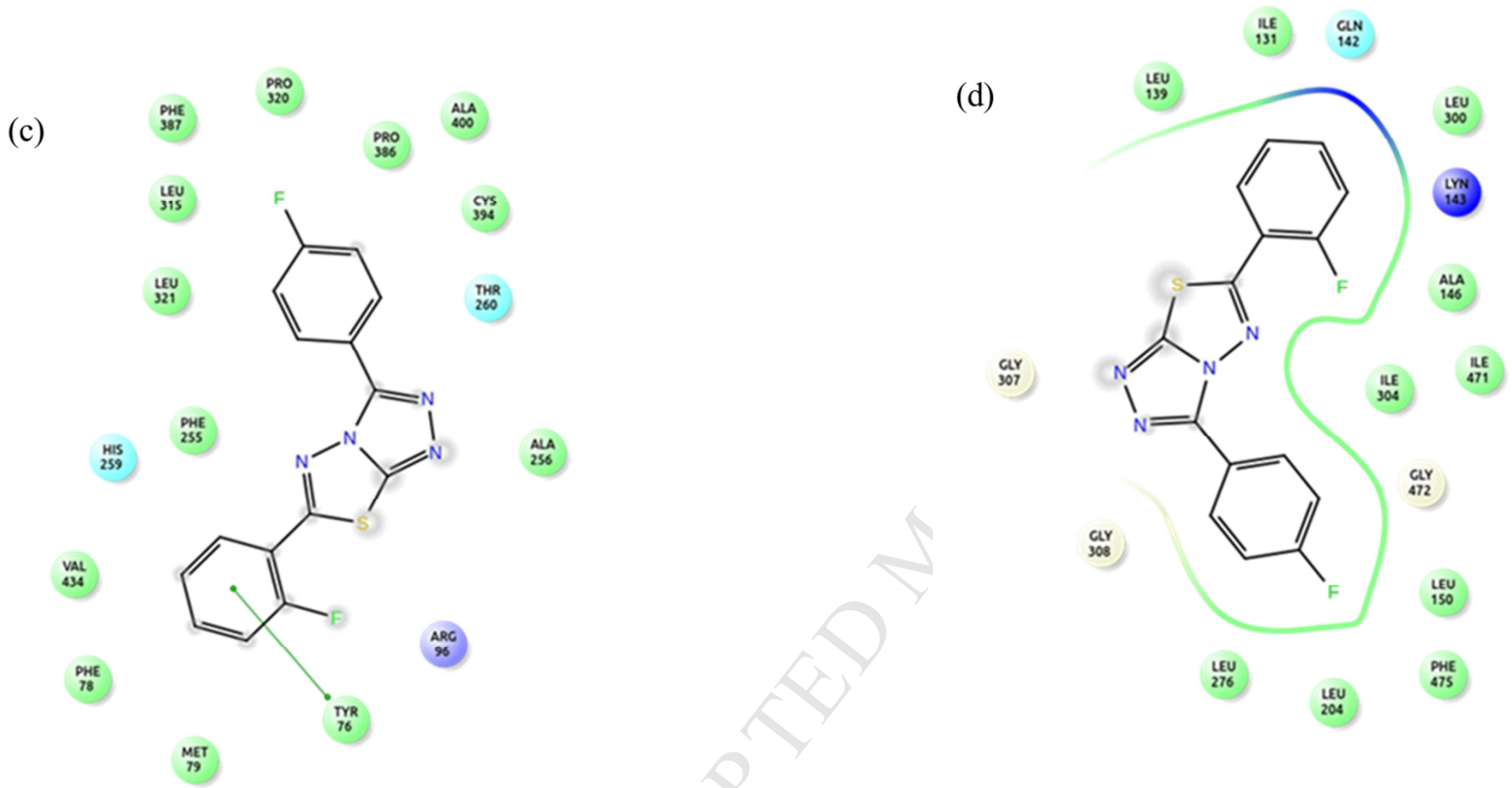

Fig. 7. Predicted binding mode of the title compound in different protein targets (a) COX-1 (b) COX-2 (c) *Mtb*CYP51 and (d) *Ca*CYP51.

4. Conclusion

In the present study, pharmaceutically promising agent, 3-(4-fluorophenyl)-6-(2-fluorophenyl)-1,2,4-triazolo[3,4-*b*][1,3,4]thiadiazole was synthesized and its single X-ray crystal diffraction analysis was performed. Two intramolecular (C–H···N and F···S) bonding are important for maintaining the planarity of the molecule at some extent and the C–H···N interaction was found to be invariant in a closely related structures. The crystal structure is stabilized by different types (molecular stacking, S··π, C–H···N, C–H··π and C–H···F interactions. Both intra and intermolecular interactions were quantified using QTAIM approach. The results suggested that the intermolecular C–H···N and C–H···F (involving F substituted at the *ortho* position) interactions play vital role in the stabilization of the crystal structure of the title compound. Other weak non-covalent interactions (S··π and π··π and N··π) also help to stabilize the crystal structure in a non-classical manner. Hirshfeld surface analysis indicated that the *para*-substituted fluorine substantially alters the contribution of intermolecular H···H and H···C contacts. The potential bioactivity of the title compound was studied by molecular docking analysis and the result revealed that the title compound may possess anti-inflammatory, antimicrobial, antifungal activities.

Acknowledgements

This work was funded by the Deanship of Scientific Research at Princess Nourah bint Abdulrahman University through the Research Group Program (Grant No. RGP-1438-0010). ST thanks the DST-SERB (SB/YS/LS-19/2014) and Prof. TRR grant for research funding. ST and MJP would like to thank Laboratorio Nacional de Supercomputo del Sureste (LNS-BUAP) for computational resources.

Competing interests

The authors declare no competing financial interest.

References

[1] H.-J. Schneider, Binding mechanisms in supramolecular complexes, Angew. Chem. Int. Ed. 48 (2009) 3924-3977.

[2] G.R. Desiraju, Crystal engineering: From molecule to crystal, J. Am. Chem. Soc. 135 (2013) 9952-9967.

[3] K. Müller-Dethlefs, P. Hobza, Noncovalent interactions: A challenge for experiment and theory, Chem. Rev. 100 (2000) 143-168.

[4] C.B. Aakeröy, N.R. Champness, C. Janiak, Recent advances in crystal engineering, CrystEngComm 12 (2010) 22-43.

[5] E. Arunan, R. Desiraju Gautam, A. Klein Roger, J. Sadlej, S. Scheiner, I. Alkorta, C. Clary David, H. Crabtree Robert, J. Dannenberg Joseph, P. Hobza, G. Kjaergaard Henrik, C. Legon Anthony, B. Mennucci, J. Nesbitt David, Defining the hydrogen bond: An account (IUPAC Technical Report), Pure and Appl. Chem., 2011, pp. 1619-1636.

[6] E. Arunan, R. Desiraju Gautam, A. Klein Roger, J. Sadlej, S. Scheiner, I. Alkorta, C. Clary David, H. Crabtree Robert, J. Dannenberg Joseph, P. Hobza, G. Kjaergaard Henrik, C. Legon Anthony, B. Mennucci, J. Nesbitt David, Definition of the hydrogen bond (IUPAC Recommendations 2011), Pure and Appl. Chem., 2011, pp. 1637-1641.

[7] G.R. Desiraju, A Bond by any other name, Angew. Chem. Int. Ed. 50 (2011) 52-59.

[8] G.R. Desiraju, T. Steiner, The weak hydrogen bond: In Structural Chemistry and Biology, Oxford University Press, 1999.

[9] I. Khan, P. Panini, S.U.-D. Khan, U.A. Rana, H. Andleeb, D. Chopra, S. Hameed, J. Simpson, Exploiting the role of molecular electrostatic potential, deformation density, topology, and energetics in the characterization of S···N and Cl···N supramolecular motifs in crystalline triazolothiadiazoles, Cryst. Growth Des. 16 (2016) 1371-1386.

[10] S. Bhandary, A. Sirohiwal, R. Kadu, S. Kumar, D. Chopra, Dispersion stabilized Se/Te··π double chalcogen bonding synthons in in situ cryocrystallized divalent organochalcogen liquids, Cryst. Growth Des. 18 (2018) 3734-3739.

[11] R. Shukla, D. Chopra, Characterization of the short O=C...O=C π-hole tetrel bond in the solid state, CrystEngComm 20 (2018) 3308-3312.

[12] L.H. Al-Wahaibi, N.S. Kumar, A.A. El-Emam, N.S. Venkataramanan, H.A. Ghabbour, A.-M.S. Al-Tamimi, J. Percino, S. Thamotharan, Investigation of potential anti-malarial lead candidate 2-(4-fluorobenzylthio)-5-(5-bromothiophen-2-yl)-1,3,4-oxadiazole: Insights from crystal structure, DFT, QTAIM and hybrid QM/MM binding energy analysis, J. Mol. Struct. 1175 (2019) 230-240.

[13] A.A. Kadi, E.S. Al-Abdullah, I.A. Shehata, E.E. Habib, T.M. Ibrahim, A.A. El-Emam, Synthesis, antimicrobial and anti-inflammatory activities of novel 5-(1-adamantyl)-1,3,4-thiadiazole derivatives, E. J. Med. Chem. 45 (2010) 5006-5011.

[14] H.N. Hafez, M.I. Hegab, I.S. Ahmed-Farag, A.B.A. El-Gazzar, A facile regioselective synthesis of novel spiro-thioxanthene and spiro-xanthene-9′,2-[1,3,4]thiadiazole derivatives as potential analgesic and anti-inflammatory agents, Bioorg. Med. Chem. Lett. 18 (2008) 4538-4543.

[15] A. Husain, M. Rashid, R. Mishra, S. Parveen, D.-S. Shin, D. Kumar, Benzimidazole bearing oxadiazole and triazolo-thiadiazoles nucleus: Design and synthesis as anticancer agents, Bioorg. Med. Chem. Lett. 22 (2012) 5438-5444.

[16] M. Amir, H. Kumar, S.A. Javed, Synthesis and pharmacological evaluation of condensed heterocyclic 6-substituted-1,2,4-triazolo[3,4-b]-1,3,4-thiadiazole derivatives of naproxen, Bioorg. Med. Chem. Lett. 17 (2007) 4504-4508.

[17] A. Reddy, S.G. Kini, M. Mubeen, Synthesis and biological evaluation of novel triazolo-thiadiazole derivatives, Der Pharma Chemica 5 (2013) 259-272.

[18] V. Mathew, J. Keshavayya, V.P. Vaidya, D. Giles, Studies on synthesis and pharmacological activities of 3,6-disubstituted-1,2,4-triazolo[3,4-b]-1,3,4-thiadiazoles and their dihydro analogues, Eur. J. Med. Chem. 42 (2007) 823-840.

[19] L. Zhang, J. Zhao, B. Zhang, T. Lu, Y. Chen, Discovery of [1,2,4]triazolo[3,4-*b*][1,3,4]thiadiazole derivatives as novel, potent and selective c-Met kinase inhibitors: Synthesis, SAR study, and biological activity, Eur. J. Med. Chem. 150 (2018) 809-816.

[20] H.-T. Du, H.-J. Du, W. Zhou, 3,6-Bis(3,4,5-trimethoxyphenyl)-1,2,4-triazolo[3,4-*b*][1,3,4]thiadiazole, Acta Crystallogr. E64 (2008) o1577.

[21] M.A. Al-Alshaikh, H.A. Ghabbour, M.S.M. Abdelbaky, S. Garcia-Granda, A.A. El-Emam, Crystal structure of 6-(2-fluorophenyl)-3-phenyl-[1,2,4]-triazolo[3,4-*b*][1,3,4]thiadiazole, C15H9FN4S, Z. Kristallogr. - New Crystal Structures 231 (2016) 661-663.

[22] H. Du, H. Du, Y. An, S. Li, 6-(2-Methylphenyl)-3-(3,4,5-trimethoxyphenyl)-1,2,4-triazolo[3,4-b][1,3,4]thiadiazole, Acta Crystallogr. E64 (2008) o1481.

[23] X.-B. Huang, M.-C. Liu, L.-X. Zhang, A.-J. Zhang, Y.-L. Xu, M.-L. Hu, 3-(2-Ethoxyphenyl)-6-phenyl-1,2,4-triazolo[3,4-b][1,3,4]thiadiazole, Acta Crystallogr. E61 (2005) o2233-o2234.

[24] H.-T. Du, H.-J. Du, W. Zhou, 6-(4-Methylphenyl)-3-(3,4,5-trimethoxyphenyl)-1,2,4-triazolo[3,4-b][1,3,4]thiadiazole, Acta Crystallographica Section E64 (2008) o2040.

[25] S. Naveen, S.N. Swamy, Basappa, B.P. Swamy, S.M. Anandalwar, J.S. Prasad, K.S. Rangappa, Crystal structure of 3-para tolyl-6-(4′-methyl-biphenyl-2-yl)-[1,2,4]triazolo[3,4-b][1,3,4]thiadiazole, Analytical Sciences: X-ray Structure Analysis Online 22 (2006) x221-x222.

[26] P. Molina, A. Arques, M.A. Alias, A.L.L. Saiz, M.D.L. Concepción Foces-Foces, Ring-opening reactions of mesoionic [1,2,4]triazolo[1,5-c]quinazolines. - Preparation

of 1,2,4-triazolo[3,4-b][1,3,4]thiadiazoles by a translocative rearrangement, Liebigs Annalen der Chemie 1989 (1989) 1055-1059.

[27] X.-X. Lei, A.-J. Zhang, X.-B. Huang, L.-X. Zhang, 6-(2-Chlorophenyl)-3-(4-ethoxyphenyl)-1,2,4-triazolo[3,4-b][1,3,4]thiadiazole, Acta Crystallogr. E62 (2006) o4418-o4419.

[28] R.F.W. Bader, A quantum theory of molecular structure and its applications, Chem. Rev. 91 (1991) 893-928.

[29] R.H. Blessing, An empirical correction for absorption anisotropy, Acta Crystallogr. A51 (1995) 33-38.

[30] G.M. Sheldrick, A short history of SHELX, Acta Crystallogr. A64 (2008) 112-122.

[31] G. Sheldrick, Crystal structure refinement with SHELXL, Acta Crystallogr. C71 (2015) 3-8.

[32] A. Spek, Structure validation in chemical crystallography, Acta Crystallogr. D65 (2009) 148-155.

[33] C.F. Macrae, P.R. Edgington, P. McCabe, E. Pidcock, G.P. Shields, R. Taylor, M. Towler, J. van de Streek, Mercury: visualization and analysis of crystal structures, J. Appl. Crystallogr. 39 (2006) 453-457.

[34] Y. Zhao, D.G. Truhlar, The M06 suite of density functionals for main group thermochemistry, thermochemical kinetics, noncovalent interactions, excited states, and transition elements: two new functionals and systematic testing of four M06-class functionals and 12 other functionals, Theor. Chem. Acc. 120 (2008) 215-241.

[35] M.J. Frisch, G.W. Trucks, H.B. Schlegel, G.E. Scuseria, M.A. Robb, J.R. Cheeseman, G. Scalmani, V. Barone, B. Mennucci, G.A. Petersson, H. Nakatsuji, M. Caricato, X. Li, H.P. Hratchian, A.F. Izmaylov, J. Bloino, G. Zheng, J.L. Sonnenberg, M. Hada, M. Ehara, K. Toyota, R. Fukuda, J. Hasegawa, M. Ishida, T. Nakajima, Y. Honda, O. Kitao, H. Nakai, T. Vreven, J.A. Montgomery Jr., J.E. Peralta, F. Ogliaro, M.J. Bearpark, J. Heyd, E.N. Brothers, K.N. Kudin, V.N. Staroverov, R. Kobayashi, J. Normand, K. Raghavachari, A.P. Rendell, J.C. Burant, S.S. Iyengar, J. Tomasi, M. Cossi, N. Rega, N.J. Millam, M. Klene, J.E. Knox, J.B. Cross, V. Bakken, C. Adamo, J. Jaramillo, R. Gomperts, R.E. Stratmann, O. Yazyev, A.J. Austin, R. Cammi, C. Pomelli, J.W. Ochterski, R.L. Martin, K. Morokuma, V.G. Zakrzewski, G.A. Voth, P. Salvador, J.J. Dannenberg, S. Dapprich, A.D. Daniels, Ö. Farkas, J.B. Foresman, J.V. Ortiz, J. Cioslowski, D.J. Fox, Gaussian 09, revision D.01, Gaussian, Inc., Wallingford, CT, USA, 2013.

[36] S. Grimme, J. Antony, S. Ehrlich, H. Krieg, A consistent and accurate ab initio parametrization of density functional dispersion correction (DFT-D) for the 94 elements H-Pu, J. Chem. Phys. 132 (2010) 154104.

[37] S.K. Wolff, D.J. Grimwood, J.J. McKinnon, M.J. Turner, D. Jayatilaka, M.A. Spackman, CrystalExplorer (Version 3.1), University of Western Australia (2012).

[38] A. Gavezzotti, Efficient computer modeling of organic materials. The atom-atom, Coulomb-London-Pauli (AA-CLP) model for intermolecular electrostatic-polarization, dispersion and repulsion energies, New J. Chem. 35 (2011) 1360-1368.

[39] A. Gavezzotti, Calculation of intermolecular interaction energies by direct numerical integration over electron densities. I. Electrostatic and polarization energies in molecular crystals, J. Phy. Chem. B 106 (2002) 4145-4154.

[40] L.H. Al-Wahaibi, S. Sujay, G.G. Muthu, A.A. El-Emam, N.S. Venkataramanan, F.A.M. Al-Omary, H.A. Ghabbour, J. Percino, S. Thamotharan, Theoretical investigations of two adamantane derivatives: A combined X-ray, DFT, QTAIM analysis and molecular docking, J. Mol. Struct. 1159 (2018) 233-245.

[41] M. Udayakumar, K. Jagatheeswaran, S.S. Ganesan, N.S. Venkataramanan, S. M. Kumar, K. Byrappa, S. Thamotharan, Investigation of 9-(2-hydroxy-4,4-dimethyl-6-oxocyclohex-1-en-1-yl)-3,3-dimethyl-2,3,4,9-tetrahydro-1H-xanthen-1-one: Crystal structure, AIM and NBO analysis, J. Mol. Struct. 1133 (2017) 510-518.

[42] P. Venkatesan, V. Rajakannan, N.S. Venkataramanan, A. Ilangovan, T. Sundius, S. Thamotharan, Structural investigation of (2E)-2-(ethoxycarbonyl)-3-[(4-methoxyphenyl)amino]prop-2-enoic acid: X-ray crystal structure, spectroscopy and DFT, J. Mol. Struct. 1119 (2016) 259-268.

[43] P. Venkatesan, S. Thamotharan, A. Ilangovan, H. Liang, T. Sundius, Crystal structure, Hirshfeld surfaces and DFT computation of NLO active (2E)-2-(ethoxycarbonyl)-3-[(1-methoxy-1-oxo-3-phenylpropan-2-yl)amino] prop-2-enoic acid, Spectrochim. Acta A 153 (2016) 625-636.

[44] P. Venkatesan, S. Thamotharan, R.G. Kumar, A. Ilangovan, Invariant and variable intermolecular interactions in functionalized malonic acid half-esters: X-ray, Hirshfeld surface and PIXEL energy analyses, CrystEngComm 17 (2015) 904-915.

[45] S. Thamotharan, J. Kothandapani, S. Selva Ganesan, N.S. Venkataramanan, S. Madan Kumar, K. Byrappa, J. Percino, F. Robles, Quantitative analysis of intermolecular interactions in 2,2'-((4-bromophenyl)methylene)bis(3-hydroxy-5,5-dimethylcyclohex-2-en-1-one): Insights from crystal structure, PIXEL, Hirshfeld surfaces and QTAIM analysis, J. Chem. Sci. 130 (2018) 20.

[46] T. Gelbrich, T.L. Threlfall, M.B. Hursthouse, XPac dissimilarity parameters as quantitative descriptors of isostructurality: The case of fourteen 4,5′-substituted benzenesulfonamido-2-pyridines obtained by substituent interchange involving CF3/I/Br/Cl/F/Me/H, CrystEngComm 14 (2012) 5454-5464.

[47] T. Gelbrich, M.B. Hursthouse, A versatile procedure for the identification, description and quantification of structural similarity in molecular crystals, CrystEngComm 7 (2005) 324-336.

[48] F.A. Bulat, A. Toro-Labbé, T. Brinck, J.S. Murray, P. Politzer, Quantitative analysis of molecular surfaces: areas, volumes, electrostatic potentials and average local ionization energies, J. Mol. Model. 16 (2010) 1679-1691.

[49] S.F. Boys, F. Bernardi, The calculation of small molecular interactions by the differences of separate total energies. Some procedures with reduced errors, Mol. Phys. 19 (1970) 553-566.

[50] T. Keith, AIMAll 16.05.18, TK Gristmill Software, 2016.

[51] E. Espinosa, E. Molins, C. Lecomte, Hydrogen bond strengths revealed by topological analyses of experimentally observed electron densities, Chem. Phys. Lett. 285 (1998) 170-173.

[52] R.A. Friesner, R.B. Murphy, M.P. Repasky, L.L. Frye, J.R. Greenwood, T.A. Halgren, P.C. Sanschagrin, D.T. Mainz, Extra Precision Glide: Docking and scoring incorporating a model of hydrophobic enclosure for protein-ligand complexes, J. Med. Chem. 49 (2006) 6177-6196.

[53] X.-B. Huang, M.-C. Liu, L.-X. Zhang, A.-J. Zhang, Y.-L. Xu, M.-L. Hu, 3-(2-Ethoxyphenyl)-6-phenyl-1,2,4-triazolo[3,4-*b*][1,3,4]thiadiazole, Acta Crystallogr. E61 (2005) o2233-o2234.

[54] E. Espinosa, I. Alkorta, J. Elguero, E. Molins, From weak to strong interactions: A comprehensive analysis of the topological and energetic properties of the electron density distribution involving X–H···F–Y systems, J. Chem. Phys. 117 (2002) 5529-5542.

[55] P.L.A. Popelier, Characterization of a dihydrogen bond on the basis of the electron density, J. Phy. Chem. A 102 (1998) 1873-1878.

[56] U. Koch, P.L.A. Popelier, Characterization of C-H-O hydrogen bonds on the basis of the charge density, J. Phy. Chem. B 99 (1995) 9747-9754.

Table 1. Crystal data and refinement parameters for the compound (**A**).

Crystal data	**A**
Chemical formula	$C_{15}H_8F_2N_4S$
*M*r	314.31
Crystal system, space group	Tetragonal, $I4_1/a$
Temperature (K)	293(2)
a, *b*, *c* (Å)	29.6253(14) 29.6253(14) 6.2433 (4)
α, β, γ(°)	90, 90, 90
V (Å^3)	5479.5(5)
Z	16
Radiation type	Mo *K*α
μ (mm^{-1})	0.26
Crystal size	0.24 × 0.12 × 0.08
Data collection	
Diffractometer	Bruker *APEX*-II CCD diffractometer
Absorption correction	Muli-scan
T_{min}, T_{max}	0.795, 0.931
No. of measured, independent and observed [$I > 2\sigma(I)$] reflections	48849, 3142, 1946
R_{int}	0.131
$(\sin\theta/\lambda)_{max}$ (Å^{-1})	0.649
Refinement	
$R[F^2 > 2\sigma(F^2)]$, $wR(F^2)$, *S*	0.048, 0.111, 1.08
No. of reflections	2513
No. of parameters	200
H-atom treatment	H-atom parameters constrained
$\Delta\rho_{max}$, $\Delta\rho_{min}$ (e Å^{-3})	0.20, -0.19
CCDC No.	1887657

Table 2

Topological parameters for intramolecular interactions in the title compound (**A**) and its closely related structures [ρ: electron density (e/Å^3), $\nabla^2\rho$: Laplacian of electron density (e/Å^5); V_b: potential energy density (a.u.), G_b: kinetic energy density (a.u.); R_{ij}: bond path (Å) and $DE_{int}= -0.5\times V_b$ in kcal mol^{-1}].

Interacting atoms	R_{ij}	ρ	$\nabla^2\rho$	V_b	G_b	$\frac{\lvert V_b\rvert}{G_b}$	DE_{int}
A							
F1···S1	2.719	0.115	1.838	-0.013541	0.016303	0.83	4.25
H15···N4	2.430	0.083	1.139	-0.007327	0.009574	0.77	2.30
ILETOK							
F1···S1	2.754	0.106	1.695	-0.012318	0.014949	0.82	3.86
H5···N2	2.395	0.089	1.228	-0.008024	0.010384	0.77	2.52
ROGGIE							
H1···N4	2.300	0.106	1.483	-0.010053	0.012722	0.79	3.15
HODNOE							
H1···N4	2.295	0.108	1.507	-0.010257	0.012946	0.79	3.22
KOFKOG							
H12···S1	2.559	0.114	1.536	-0.012361	0.014147	0.87	3.88
H1···N4	2.402	0.088	1.209	-0.007823	0.010181	0.77	2.45
LEPQED							
Cl1···S1	3.002	0.128	1.531	-0.013332	0.014606	0.91	4.18
H5···N1	2.494	0.076	1.038	-0.006635	0.008701	0.76	2.08
VEGVAE							
H4···N4	2.308	0.105	1.451	-0.009945	0.012501	0.80	3.12
XERZUG							
C17···S1	3.035	0.096	1.098	-0.009004	0.010196	0.88	2.83
H4···N2	2.447	0.082	1.116	-0.007182	0.009380	0.77	2.25

Table 3. Interaction energy (in kcal mol^{-1}) for various molecular pair along with centroid-centroid distance in (I). *Cg*1 and *Cg*3 are the centroids of the 2-fluorophenyl and 4-fluorophenyl rings, respectively.

Motifs	**centroid-centroid distance (Å)**	**Symmetry code**	E_{Coul}	E_{pol}	E_{disp}	E_{rep}	E_{tot}	ΔE_{CP}	**Possible Interactions**	**Geometry (Å,°)[a]**
I	5.943	–x, –y, –z+1	–3.9	–1.9	–11.1	7.7	–9.2	–10.3	Molecular stacking C9···N1 (*Cg*3···*Cg*3)	 3.246(3) 3.317(3)
II	6.243	x, y, z–1	–1.5	–1.1	–13.0	7.2	–8.4	–10.3	Molecular stacking C5···C10 (*Cg*1···*Cg*3)	 3.353(4) 3.664(4)
III	9.714	–x, –y, –z+2	–5.0	–2.9	–5.4	6.2	–7.1	–6.4	C11–H11···N2	2.39, 165
IV	8.718	–y+1/4,x+1/4, –z+1/4	–3.7	–1.2	–5.1	5.1	–4.9	–6.0	S1···C3 S1···C4	3.457(3) 3.486(3)
V	9.364	–y–1/4,x+1/4, z–3/4	–1.2	–0.5	–4.7	2.2	–4.3	–4.1	C5–H5···C13	2.86, 130
VI	12.385	–y+1/4,x+1/4, –z–3/4	–0.5	–0.3	–2.2	1.1	–1.9	–1.6	C2–H2···F1 C3–H3···F1	2.63, 116 2.63, 116

[a]Neutron values are given for all D–H···A interactions.

Table 4. Topological parameters for selected molecular pairs (I to VI) in the compound (**A**) [ρ: electron density (e/Å^3), $\nabla^2\rho$: Laplacian of electron density (e/Å^5); V_b: potential energy density (a.u.), G_b: kinetic energy density (a.u.); R_{ij}: bond path (Å) and DE_{int}= –0.5×V_b in kcal mol^{-1}].

Interacting atoms	R_{ij}	ρ	$\nabla^2\rho$	V_b	G_b	$\frac{\lvert V_b\rvert}{G_b}$	DE_{int}
I							
N1···C9	3.643	0.042	0.492	-0.003042	0.004074	0.75	0.95
C9···N1	3.643	0.042	0.492	-0.003042	0.004074	0.75	0.95
N2···N3	3.335	0.035	0.480	-0.002943	0.003960	0.74	0.92
N3···N3	3.335	0.035	0.480	-0.002943	0.003960	0.74	0.92
II							
C3···N4	3.697	0.037	0.410	-0.002263	0.003261	0.69	0.71
C5···C10	3.655	0.041	0.438	-0.002267	0.003404	0.67	0.71
C6···N2	4.114	0.033	0.404	-0.002001	0.003094	0.65	0.63
C11···N4	3.602	0.024	0.297	-0.001581	0.002332	0.68	0.50
III							
H11···N2	2.415	0.069	1.028	-0.007008	0.008835	0.79	2.20
N2···H11	2.415	0.069	1.028	-0.007008	0.008835	0.79	2.20
IV							
H3···N1	2.917	0.045	0.644	-0.003954	0.005315	0.74	1.24
S1···C3	3.684	0.040	0.502	-0.002903	0.004054	0.72	0.91
S1···C4	3.542	0.034	0.481	-0.002769	0.003882	0.71	0.87
V							
H15···F2	2.811	0.023	0.385	-0.002534	0.003262	0.78	0.80
H5···C13	2.944	0.026	0.397	-0.002255	0.003188	0.71	0.71
H4···C14	3.026	0.029	0.377	-0.002180	0.003045	0.72	0.68
H14···F2	2.942	0.017	0.325	-0.001905	0.002640	0.72	0.60
VI							
H3···F1	2.701	0.038	0.636	-0.004387	0.005492	0.80	1.38
H2···F1	2.727	0.036	0.593	-0.004071	0.005110	0.80	1.28

Table 5. The binding energies (in kcal mol^{-1}) for the compound **(A)** and control inhibitors calculated by Glide XP scoring scheme

Compound	Target			
	O.aries COX-1	*H. sapiens* COX-2	*M.tuber*culosis CYP51	*C.albicans* CYP51
A	**-8.953**	**-7.906**	**-7.138**	**-7.612**
Mefanamic acid		-3.813	---	---
Ibuprofen	-8.525	---	---	---
Fluconazole	---	---	-1.964	-2.727

HIGHLIGHTS

- Molecule forms as pseudo 6, 5, 5, 5, 6, 6-membered ring system.
- The invariant intramolecular C–H···N interactions are quantified.
- Topological properties of intermolecular interactions are given
- Different bioactivities are explored using molecular docking.
- Role of fluorine in the crystal is investigated.